Charlotte D. Vacogne | Sarah M. Brosnan | Admir Masic
Helmut Schlaad

Fibrillar gels via the self-assembly of poly(L-glutamate)-based statistical copolymers

Suggested citation referring to the original publication:
Polym. Chem. 6 (2015), pp. 5040–5052
DOI http://dx.doi.org/10.1039/C5PY00491H
ISSN (print) 1759-9954
ISSN (online) 1759-9962

Polymer Chemistry

PAPER

View Article Online
View Journal | View Issue

Cite this: *Polym. Chem.*, 2015, **6**, 5040

Fibrillar gels *via* the self-assembly of poly(L-glutamate)-based statistical copolymers†

Charlotte D. Vacogne,[a] Sarah M. Brosnan,[a] Admir Masic[b] and Helmut Schlaad*[c]

Received 1st April 2015,
Accepted 12th May 2015

DOI: 10.1039/c5py00491h

www.rsc.org/polymers

Polypeptides having secondary structures often undergo self-assembly which can extend over multiple length scales. Poly(γ-benzyl-L-glutamate) (PBLG), for example, folds into α-helices and forms physical organogels, whereas poly(L-glutamic acid) (PLGA at acidic pH) or poly(L-glutamate) (PLG at neutral/basic pH) do not form hydrogels. We explored the gelation of modified PBLG and investigated the deprotection of the carboxylic acid moieties in such gels to yield unique hydrogels. This was accomplished through photo-crosslinking gelation of poly(γ-benzyl-L-glutamate-*co*-allylglycine) statistical copolymers in toluene, tetrahydrofuran, and 1,4-dioxane. Unlike most polymer-based chemical gels, our gels were prepared from dilute solutions (<20 g L^{-1}, *i.e.*, <2% w/v) of low molar mass polymers. Despite such low concentrations and molar masses, our dioxane gels showed high mechanical stability and little shrinkage; remarkably, they also exhibited a porous fibrillar network. Deprotection of the carboxylic acid moieties in dioxane gels yielded pH responsive and highly absorbent PLGA/PLG-based hydrogels (swelling ratio of up to 87), while preserving the network structure, which is an unprecedented feature in the context of crosslinked PLGA gels. These outstanding properties are highly attractive for biomedical materials.

Introduction

Polypeptide-based hydrogels are becoming increasingly important biomedical materials[1–4] as they provide a biomimetic, porous, and hydrophilic environment, ideal to support cell colonisation[5] and drug delivery.[4,6] There are many examples of hydrogels used in medicine derived from natural polypeptides, such as soluble collagen,[7] gelatin,[8,9] and fibrin.[10] Due to their natural origin, such polypeptides have predefined structures, compositions, and sequences,[11] which while confers potential advantages like biocompatibility and bioactivity, fundamentally limits the extent by which they can be chemically modified or, more critically, processed to fit specific needs of the application. One way to overcome these limitations is the use of synthetic polypeptides, as they can be easily tailored to offer a variety of chain lengths, compositions (*e.g.*, sequence controlled, block or random copolymers, and natural or non-natural amino acids) and secondary structures (*e.g.*, α-helices and β-sheets). Non-sequence controlled synthetic polymer often represent a biocompatible alternative to expensive biosourced polypeptides or proteins, such as collagen.[12] Owing to their secondary structure, these polymers can behave as macromolecular building blocks and self-assemble to form supramolecular assemblies (*e.g.*, fibers, gels, or liquid crystals).[1–3,13] In particular, self-assembled polypeptide hydrogels offer competitive advantages in the search for biomedical gels:[14,15] supramolecular assembly of carefully selected polypeptides can yield fibrillar gels,[16] synthetic polypeptides can be tailored to tune the gel properties (*e.g.*, density, porosity, and microstructure), in turn yielding higher swelling ratios than crosslinked hydrogels or blends;[17–23] and finally, the composition of such supramolecular building blocks can be tuned to offer intrinsically biocompatible and easily biodegradable polymers. As such, synthetic polypeptides offer a versatile approach towards structural[24] and stimuli-responsive[9,25] medical hydrogels.[26]

Typically, sequence-controlled polypeptides are synthesized by solid phase synthesis.[27] The advantage of this technique is the complete control over the polypeptide sequence and chain length, thereby yielding biomimetic macromolecules; however, this technique produces polypeptides in small quantities (<1 g) and with low degree of polymerization (<50 repeat units). A cost effective route for the synthesis of longer polypeptides in larger quantities is ring opening polymerization (ROP) of α-amino acid *N*-carboxyanhydride (NCA). Poly(γ-benzyl-L-glutamate) (PBLG) is one of the most common poly-

[a]*Max Planck Institute of Colloids and Interfaces, Department of Colloid Chemistry, Research Campus Golm, 14424 Potsdam, Germany*
[b]*Max Planck Institute of Colloids and Interfaces, Department of Biomaterials, Research Campus Golm, 14424 Potsdam, Germany*
[c]*University of Potsdam, Institute of Chemistry, Karl-Liebknecht-Straße 24-25, 14476 Potsdam, Germany. E-mail: schlaad@uni-potsdam.de*
†Electronic supplementary information (ESI) available. See DOI: 10.1039/c5py00491h

peptides synthesized by ROP.[1,28] Additionally, the carboxylic acid moieties of PBLG can be debenzylated to yield its biocompatible counterpart, poly(L-glutamic acid) (PLGA, hydrophobic) at acidic pH and poly(L-glutamate) (PLG, hydrophilic) at neutral and basic pH.[29–31] The popularity of PBLG and PLGA can be attributed to a relatively inexpensive α-amino acid precursor, L-glutamic acid γ-benzyl ester, and also to their ability to fold into α-helices. PLGA undergoes a helix-to-coil transition at acidic pH (*ca*. pH 5–6), making it an attractive candidate for stimuli-responsive bio-systems.[1,32–36] Notably, the rod-like α-helical conformation,[25,37] pH-responsiveness[36–40] and good solubility at neutral and high pH[13] of PLGA and PLG have been exploited in block copolymers used for vesicles and hydrogels. PLGA and PLG, however, do not self-assemble into physical hydrogels: while the hydrophobicity of PLGA α-helices causes them to precipitate from water, PLG chains only exist as random coils in water.[41] The formation of long range order or supramolecular assemblies from α-helical building blocks in water is challenging as water disrupts hydrogen bonds, essential to the stabilization of secondary structures.[4,42] That is why PLGA-based hydrogels are generally prepared by (i) chemical crosslinking using water soluble carbodiimides[17] or diamines,[18,19] (ii) blending with cationic polymers,[20,21] (iii) self-assembly of PLGA-based block copolymers,[21] and (iv) lyophilization.[17] None of the aforementioned gels result from the self-assembly of PLGA α-helices.

Unlike PLGA, PBLG α-helices can assemble in a head-to-tail and side-by-side fashion[28,43,44] and generate long range order in helicogenic organic solvents. At high concentrations (over 10 wt%), PBLG self-assembly yields lyotropic phases.[45] In dilute systems (down to 0.1 wt%) and in 'poor' solvents, such as toluene, benzyl alcohol, and dioxane–water mixtures,[46] PBLG self-assembly yields interpenetrating solvent-trapping fibers, which results in physical organogels.[45,46] Although contrasting mechanisms have been proposed for the gelation of PBLG, including (i) phase separation by spinodal decomposition, (ii) nucleation growth, and (iii) a combination of both mechanisms, the result is the formation of a percolated network of fibers.[44,47,48] The stability of PBLG helices and fibers is often attributed to a combination of the following features: intra-molecular hydrogen bonding (especially in aprotic solvents),[11] dipole–dipole interaction of the PBLG helices (especially in non-polar solvents),[43,49,50] and π–π stacking of the outward-pointing pendant benzyl groups.[51] Such organogels present attractive features, including a robust fibrous network and a high porosity,[46] which would be valuable in the context of biomedical hydrogels. It should be noted that secondary structure-driven gelation is also very common for β-sheets, which self-assemble upon extra-molecular hydrogen bonding.[52] Inspired by PBLG supramolecular assemblies, a few studies circumvented the challenging self-assembly of PLGA in water by chemically crosslinking PBLG when self-assembled into lyotropic phases to yield liquid crystalline (LC) gels, followed by debenzylation of the carboxylic acid moieties.[25,26] The highly concentrated solutions used (25 wt%) typically led to dense gels with low porosity and swelling,[18] and the crosslinking treatment, which reacted multifunctional amines with benzyl ester side groups, was extremely time-consuming (>3 days) and lacked of control over the position and number of crosslinks.[18,19,53]

In order to overcome these obstacles and achieve biocompatible fibrillar networks, we have developed a novel organogel-to-hydrogel route to prepare highly absorbent, porous, and stimuli-responsive PLGA/PLG hydrogels. This was accomplished by the synthesis by NCA ROP of statistical copolymers[54] of BLG and allylglycine (AG) of relatively low molar masses (*i.e.*, down to 11 kDa), and their photo-crosslinking gelation followed by the deprotection of the carboxylic acid moieties. BLG was chosen as the primary monomer in order to ensure α-helical conformation, and AG as the co-monomer, as it can be functionalized or crosslinked under UV using fast and quantitative thiol–ene click chemistry.[41,55,56] We report the ability for dilute solutions of our copolymers in 1,4-dioxane, toluene, and THF (down to 10 g L^{-1}, *i.e.*, 1% w/v) to form robust and highly porous UV-crosslinked organogels. We demonstrate that the self-assembly of our α-helical statistical copolymers into supramolecular fiber-like aggregates is essential for the photo-crosslinking gelation of such dilute solutions. We show that our copolymer-dioxane organogels can undergo debenzylation of their carboxylic acid moieties to yield pH-responsive and highly absorbent microfibrillar hydrogels.

Experimental

Materials

The amino acids (NCA precursors), γ-benzyl-L-glutamate (BLG) (99%) and L/DL-allylglycine (AG) (98%) were purchased from Sigma-Aldrich and BoaoPharma, respectively. Anhydrous *N*,*N*-dimethylformamide (DMF) (99.8%), 1,4-dioxane (99.8%), 1-hexylamine (99%), hydrobromic acid (37% in acetic acid), benzophenone (99%), 1,9-nonanedithiol (95%), α-pinene (98%), and methanesulfonic acid (MSA) (99.5%) were purchased from Sigma-Aldrich and used as such unless mentioned otherwise. Triphosgene and pH 4 (citric acid/sodium hydroxide/hydrogen chloride) and pH 10 (boric acid/potassium chloride/sodium hydroxide) buffer solutions were purchased from Merck. Trifluoroacetic acid (TFA) was purchased from Roth. Anhydrous tetrahydrofuran (THF) was purchased from VWR. 1-Hexylamine was distilled before use.

Polypeptide synthesis

PBLG and copolymers of BLG and AG were synthesized by polymerization of mixtures of α-amino acid *N*-carboxyanhydride (NCA). Typically, BLG-NCA (2 g, 7.6 mmol, x equiv.) and AG-NCA co-monomers ($1 - x$ equiv.), synthesized as described earlier,[41] were dried under high vacuum for 1 h and dissolved in 40 mL of dry DMF under argon in a flame-dried flask. The mixture was cooled down in ice for 20 min and the initiator solution (0.1 M 1-hexylamine in DMF, $1/n$ equiv.) was added. The reaction flask was then evacuated (1 mbar) and stirred at room temperature for 3 days. Polymerization was terminated

by addition of acetic anhydride (>50n equiv.), stirred for another 20 min and then precipitated in cold methanol. The product was collected by centrifugation and dried under high vacuum for 12 h, and lyophilized from 1,4-dioxane.

Gel preparation

Thermoreversible gels were prepared by dissolving polypeptides in toluene (1 to 50 g L^{-1}, *i.e.*, 0.1 to 5% w/v) at 60 °C for 45–60 min and cooling the mixture down to room temperature or below. In order to prepare crosslinked P(BLG-*co*-AG) gels, polypeptides were dissolved in toluene, THF or 1,4-dioxane (typically 10 to 50 g L^{-1}, *i.e.*, 1 to 5% w/v) at 60 °C in a glass vial. Crosslinker 1,9-nonanedithiol (typically 0.75 eq. relative to AG units) and type II bimolecular photoinitiator benzophenone (1 g L^{-1}) were then added. The mixture was then argon- or nitrogen-purged for 10 min and exposed to UV radiation (Heraeus TQ 150 Hg-lamp, 150 W) for 20 to 180 min, depending on the sample. In the case of 'cold-crosslinked' toluene gels, the vials were plunged in a −77 °C cooling bath and positioned upside-down to ensure UV-exposure through the bottom glass wall of the vials. In order to prepare hydrogels, dioxane gels were dried under high vacuum and immersed in a TFA/anisole/MSA (45 : 10 : 45 vol%) solution (deprotection route A) or in a TFA/HBr (75 : 25 vol%) solution (deprotection route B); 1 mL of solution per 20 mg of dried organogel. The mixtures were gently shaken in ice for 30 min and then at room temperature for another 30 min. The gels were washed with diethyl ether and immersed in an excess of $NaHCO_3$ saturated aqueous solution for 12 h. The gels were then dialyzed against distilled water for 48 h.

In order to quantify their swelling ratio (SR), the hydrogels were weighed following the debenzylation stage, in their swollen state (*i.e.*, loaded with Millipore water), as well as after the freeze-drying stage. The swelling ratio was then calculated using the following equation, $SR = (m_s - m_d)/m_d$, with m_s as the mass of the swollen hydrogel and m_d as its dry mass.

Analytical instrumentation and methods

Proton nuclear magnetic resonance (^{1}H-NMR) spectra were recorded on a Bruker DPX-400 spectrometer (400 MHz) in deuterated trifluoroacetic acid (TFA-d) for the polypeptide analysis and in deuterated toluene (toluene-d_8) for the gelation experiments. Unless mentioned otherwise, the line broadening (lb) value was set to 1.0, the number of scans was at least 128, and the acquisition time was set to 2 s.

Size exclusion chromatography (SEC) with simultaneous UV and RI detection was performed in a solution of *N*-methyl-2-pyrrolidone (NMP) with 0.5 wt% LiBr at a flow rate of 0.8 mL min^{-1} at 70 °C, on PSS-GRAM columns (7 μm particle size, 100 and 1000 Å porosity). Polymer solutions were of 1.5 mg mL^{-1}; PMMA standards (PSS, Mainz, Germany; mass range, M_p 505 to 898 000 g mol^{-1}) were used.

Fourier transform infra-red spectroscopy (FTIR) was performed on a Nicolet IS5 FTIR spectrometer (Thermo Scientific) in ATR (iD5) mode. Atmospheric background was automatically subtracted. The raw transmission spectra were converted into absorption spectra for easier post-processing and reading purposes. The spectra were baseline corrected and normalized using OMNIC™ series software. When applicable, residual atmospheric peaks were removed using the software's ad-hoc function.

Raman spectroscopy was performed on a UHTS 300 (WITec, Ulm, Germany) equipped with a Nd:YAG laser (λ = 532 nm) and a piezoscanner (P-500, Physik Instrumente, Karlsruhe, Germany) were used. The spectra were acquired with a CCD detector (DU401-BV, Andor, Belfast, UK) placed behind a grating spectrograph (1800 groves per mm, UHTS 300, WITec, Ulm, Germany). The laser beam was focused through a 10× (Nikon, NA = 0.2) microscope objective. ScanCtrlSpectroscopyPlus software (version 1.38, Witec) was used for measurement and OPUS 7.0 for spectra processing. Unless mentioned otherwise, the spectra presented in this study were narrowed down to the [1620–1720 cm^{-1}] range, baseline corrected (straight line coupled with additional concave rubberband correction – 2 iterations), smoothed (number of smoothing point 7), normalized and deconvoluted using the Levenberg–Marquardt algorithm and assuming Gaussian distributions.

Wide angle X-ray scattering (WAXS) was performed on a Nanostar X-ray diffractometer (Bruker AXS) operating at 40 kV and 35 mA (Cu Kα radiation, λ = 1.5418 Å) was used for our scattering measurements. Unless mentioned otherwise, gel and polymer samples were placed in a sealed borosilicate glass capillary (about 1.5 mm diameter), normal to the X-ray beam path. The sample-to-detector distances used were about 8 and 5 cm. The beam center and exact distance were calculated using a corundum standard. The scattering patterns were collected during 7200s of exposure time per sample and recorded by a position sensitive area 2D detector (HI-STAR, Bruker AXS, Karlsruhe, Germany). The 2D patterns were then integrated using Bruker AXS SAXS-offline software (V4.1.16) and analyzed using OriginPro (8.6G).

Scanning electron microscopy (SEM) images were taken with a Leo 1550 Gemini (Carl Zeiss AG, Germany) microscope operating at 5 to 10 kV. The samples were loaded on carbon-coated stubs and sputtered with gold palladium alloy prior to imaging.

Transmission electron microscopy (TEM) was performed on a EM 912 Omega microscope (Zeiss AG) operating at an accelerating voltage of 120 kV. The TEM gel samples were prepared by dabbing 200 mesh carbon-coated copper grids onto the gels and leaving the grids to dry under laminar air flow.

Results and discussion

Polymer synthesis

With the intention of making versatile polypeptide gels, we synthesized statistical copolymers of γ-benzyl-L-glutamate

(BLG) and allylglycine (AG). The BLG units were selected to promote α-helical conformation, and the AG units were selected for their ability to be functionalized or crosslinked by thiol–ene chemistry. α-Amino acid *N*-carboxyanhydride (NCA) monomers of BLG and AG were mixed in BLG to AG ratios ranging from 70 : 30 to 90 : 10 and polymerized by NCA ring opening polymerization (ROP) to yield poly(γ-benzyl-L-glutamate-*co*-allylglycine). For easier reading, these polymers are noted $P(BLG_x\text{-}co\text{-}AG_{1-x})_n$, with x as the BLG/(BLG + AG) mole fraction and n as the number of repeat units. Debenzylated $P(BLG_x\text{-}co\text{-}AG_{1-x})_n$ copolymers are noted $P(LG_x\text{-}co\text{-}AG_{1-x})_n$. In order to distinguish between LAG and DLAG repeat units, corresponding copolymers are noted $P(BLG_x\text{-}co\text{-}LAG_{1-x})_n$ and $P(BLG_x\text{-}co\text{-}DLAG_{1-x})_n$ respectively, and only enantiomerically pure BLG repeat units were used; the L enantiomer was chosen for its cost-effectiveness. In order to investigate novel routes to prepare organogels from dilute solutions of $P(BLG_x\text{-}co\text{-}AG_{1-x})_n$ and deprotect their carboxylic acid moieties to yield hydrogels, as depicted in Scheme 1, we synthesized a series of $P(BLG_x\text{-}co\text{-}AG_{1-x})_n$ copolymers. In this series, we varied molar masses, BLG to AG ratios and the stereochemistry of AG in order to elucidate the most suitable candidates for gelation (Table 1). For each polymer, the degree of polymerization and composition were assessed by ^{1}H-NMR (Fig. S1a–S6a†). We obtained $P(BLG_x\text{-}co\text{-}AG_{1-x})_n$ copolymers in good yield (typically over 85%) and in a controlled fashion (dispersity, $M_w/M_n < 1.3$) (Table 1).

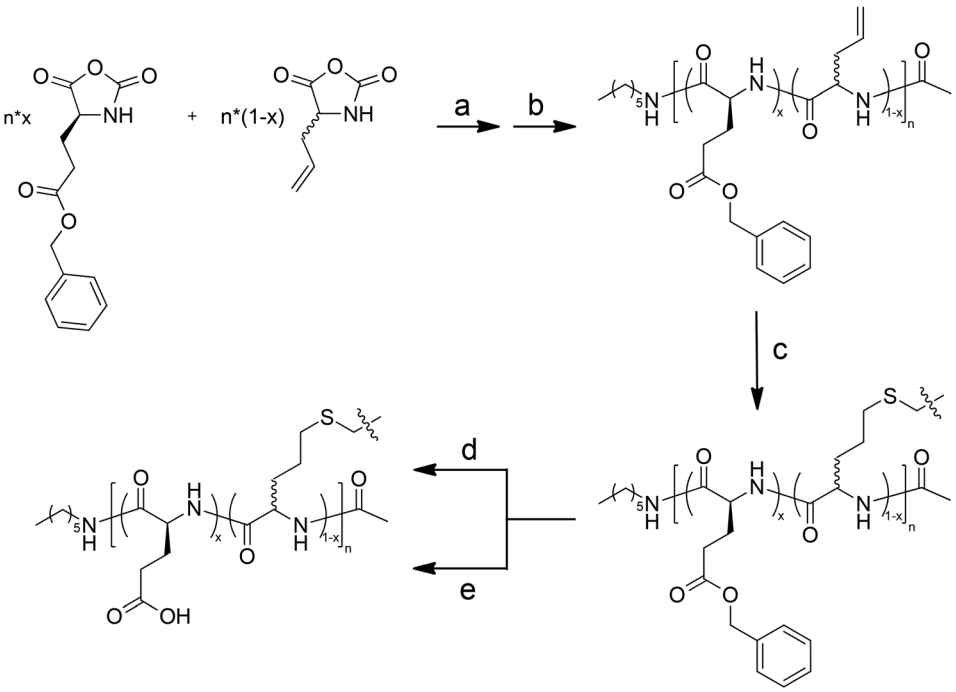

Scheme 1 Synthetic route for preparing PLGA-based hydrogels; (a) DMF, 1-hexylamine (1/*n* equiv.); (b) Ac_2O; (c) 1,4-dioxane, 1,9-nonanedithiol, benzophenone, *hν*; (d) TFA, MSA, anisole (deprotection route A); (e) TFA, HBr (37% in acetic acid) (deprotection route B).

Table 1 Molecular characteristics of (*co*)polypeptides[a,b]

	γ-Benzyl-L-glutamate (BLG)		Allyl glycine (AG)				
Polymer	Mole fraction[a]	Configuration	Mole fraction[a]	Configuration	M_n[c] (kg mol^{-1})[a]	DP[d,a]	M_w/M_n[e,b]
$PBLG_{51}$	100%	L	—	—	11.3	51	1.09
$P(BLG_{0.89}\text{-}co\text{-}DLAG_{0.11})_{53}$	89%	L	11%	DL	11.0	53	1.18
$P(BLG_{0.76}\text{-}co\text{-}DLAG_{0.24})_{59}$	76%	L	24%	DL	11.4	59	1.16
$P(BLG_{0.77}\text{-}co\text{-}LAG_{0.23})_{57}$	77%	L	23%	L	11.1	57	1.25
$P(BLG_{0.74}\text{-}co\text{-}LAG_{0.26})_{91}$	74%	L	26%	L	17.2	91	1.21
$P(BLG_{0.74}\text{-}co\text{-}LAG_{0.26})_{170}$	74%	L	26%	L	31.9	170	1.28

[a] Determined by ^{1}H-NMR (Fig. S1a–S6a). [b] Determined by SEC using PMMA calibration (Fig. S1b–S6b). [c] Number-average molar mass. [d] Number-average degree of polymerization. [e] Dispersity = ratio of weight- over number-average molar mass.

Physical gelation

The first step to synthetic polypeptide hydrogels derived from organogels was to assess the ability of our P(BLG$_x$-*co*-AG$_{1-x}$)$_n$ copolymers to form a physical gel. To do so, we studied P(BLG$_x$-*co*-AG$_{1-x}$)$_n$-toluene systems, and more specifically we focused on dilute systems in order to target high solvent content gels. Physical gelation of our polymer-toluene systems was determined by vial inversion tests and by rheological response to mechanical disruption. In addition to being a helicogenic solvent, toluene is also a poor solvent for PBLG, which enabled us to prepare physical gels by cooling heated toluene solutions of PBLG$_{51}$ below their gelation temperature, which varied depending on the polymer concentration. Typically, PBLG$_{51}$-toluene solutions of more than 10 g L^{-1} (*i.e.*, 1% w/v) formed gels at room temperature and above; for solutions below 10 g L^{-1}, gelation was substantially slower (>12 h) but could be accelerated by bringing the temperature down, which supports the coexistence of two mechanisms for the gelation of rod-like polymers: nucleation growth and phase separation.[57] Regardless, such gelation essentially results from the formation of a network of solvent-trapping fibers, which are composed of self-assembled rod-like PBLG α-helices, arranged in a head-to-tail and side-by-side fashion (Fig. 1). None of our statistical copolymers (Table 1) gelled in toluene at room temperature even for concentrations as high as 50 g L^{-1} (*i.e.*, 5% w/v). Interestingly, after maintaining the temperature of the solutions at −35 °C for only a few minutes, we observed reversible physical gelation for all P(BLG$_x$-*co*-AG$_{1-x}$)$_n$-toluene systems (10 to 50 g L^{-1}), with exception of P(BLG$_{0.76}$-*co*-DLAG$_{0.24}$)$_{59}$. This reversible thermogelation indicates that our copolymers behave similarly to PBLG in toluene. In order to find out whether the gelation of our copolymers, composed of over 74 mol% of BLG units, and of PBLG homopolymer are driven by a similar mechanism, that is the self-assembly of α-helices, we studied the secondary structure of our copolymers.

To assess the secondary structure of our copolymers, we used Raman spectroscopy (see the spectra in Fig. 2), which is an established technique for identifying and quantifying secondary structures in proteins.[58] In particular, the position of the Amide I band (ranging from 1620 to 1680 cm^{-1}), which is assigned to the C=O stretch of the amide group, is indicative of the conformation of the polypeptide. Upon deconvolution of the overlapping peaks in the Amide I range, we were able to identify two peaks and quantify their respective contribution to the overall conformation of our polymers. The Raman spectrum of PBLG$_{51}$ shows a single peak corresponding to an α-helical conformation (1652 cm^{-1}), while the spectra of our P(BLG$_x$-*co*-AG$_{1-x}$)$_n$ polypeptides consist of a mixture of a similar α-helix peak (1652 to 1655 cm^{-1}) and another peak at ~1643 cm^{-1} (Fig. 2 and Table 2). Former studies have demonstrated that in statistical copolymers of BLG and L/DL-AG, the AG units acted as defects and that the overall secondary structure of the statistical copolymer was driven by that of the BLG units (in the majority), *i.e.*, α-helical;[55] this, despite the fact that P(DLAG) homo- or block co-polymers are known to form β-sheets.[22,59] The driving force of BLG for the α-helical conformation was also demonstrated in other statistical copolymers of similar BLG to co-monomer (*e.g.*, propargylglycine) ratios.[54] For these reasons, we concluded that AG units behave as 'defects', thereby disrupting the formation of a BLG-driven homogeneous α-helical copolymer. The peak at 1643 cm^{-1} was thus ascribed to a random coil conformation, also referred to as disorder. We also found that for similar AG to BLG ratio and similar degree of polymerization (DP), the α-helical contribution is the largest when enantiomerically pure LAG is used. These observations are in agreement with CD spectroscopy studies formerly undertaken by our group on similar systems.[41] In addition, P(BLG$_{0.76}$-*co*-DLAG$_{0.24}$)$_{59}$, whose secondary structure exhibited the largest random coil contribution amongst all of our copolymers, did not gel in toluene at any of the investigated temperatures. This suggests that large DLAG to

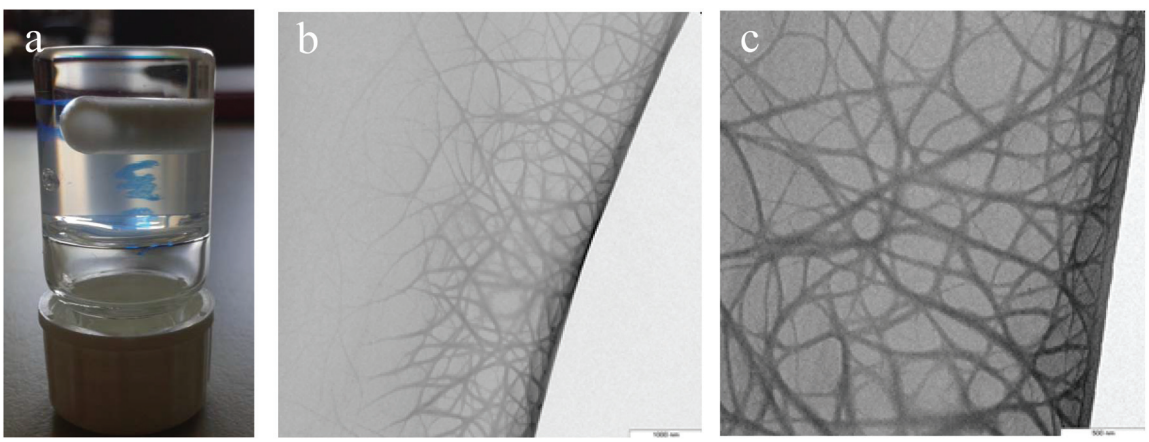

Fig. 1 Organogels of PBLG$_{51}$ in toluene: (a) vial inversion and (b, c) transmission electron micrographs of a 40 g L^{-1} gel; scale bar (b) 1000 nm, (c) 500 nm.

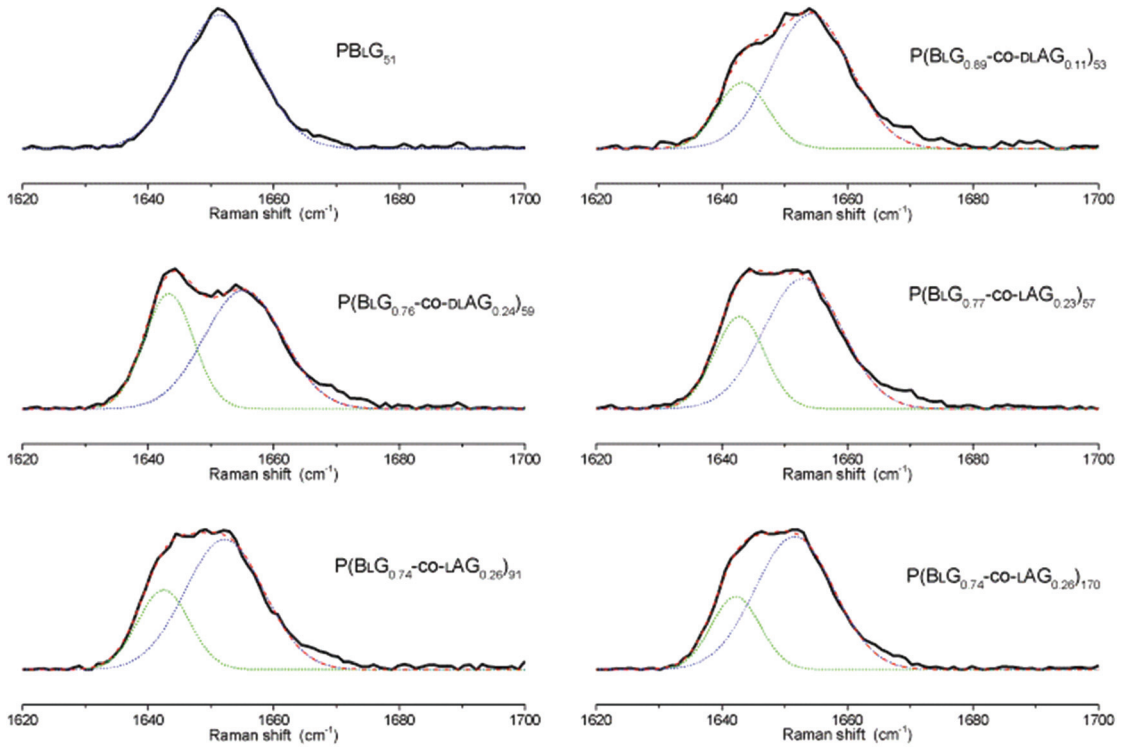

Fig. 2 Raman spectra of dry $P(BLG_x\text{-}co\text{-}AG_{1-x})_n$ polymers. Deconvoluted Amide I bands after baseline correction, smoothing, normalization, and curve-fitting using the Levenberg–Marquardt algorithm (Fig. S7†).

Table 2 Determination of secondary structure of $P(BLG_x\text{-}co\text{-}AG_{1-x})_n$ polymers based on the deconvolution of Raman Amide I bands (see Raman spectra in Fig. 2)

	Amide I – random coil		Amide I – α-helix	
Polymer	Peak position (cm^{-1})	Area under curve	Peak position (cm^{-1})	Area under curve
$PBLG_{51}$	—	—	1652	100%
$P(BLG_{0.89}\text{-}co\text{-}DLAG_{0.11})_{53}$	1643	24%	1654	76%
$P(BLG_{0.76}\text{-}co\text{-}DLAG_{0.24})_{59}$	1643	38%	1655	62%
$P(BLG_{0.77}\text{-}co\text{-}LAG_{0.23})_{57}$	1643	31%	1653	69%
$P(BLG_{0.74}\text{-}co\text{-}LAG_{0.26})_{91}$	1643	29%	1652	71%
$P(BLG_{0.74}\text{-}co\text{-}LAG_{0.26})_{170}$	1642	25%	1652	75%

BLG ratios (at least 24 : 76) prevent gelation entirely; however, the fact that $P(BLG_{0.89}\text{-}co\text{-}DLAG_{0.11})_{53}$ was able to gel shows that sufficiently low DLAG to BLG ratios (less than 24 : 76 and at least up to 11 : 89) does not prevent physical gelation. We also found that for similar LAG to BLG ratios, the α-helical contribution increases with increasing chain length. We concluded that the dominant α-helical contribution in most of our copolymers promotes rod-like behavior, which is responsible for self-assembly and physical gelation in toluene, but that the presence of AG units in our copolymers is responsible for a certain degree of disorder, particularly when AG units are non-enantiomerically pure, which in turn impedes the physical gelation by lowering the gelation temperature or preventing the gelation entirely. These depressed gelation temperatures are most likely the consequence of imperfect or less stiff $P(BLG_x\text{-}co\text{-}AG_{1-x})_n$ rods, in comparison with PBLG rods, which is the result of a disrupted α-helical secondary structure caused by the presence of AG-induced defects.

In order to get a deeper insight of the nature of the gelation and further support our observations and Raman results, we conducted ^{1}H-NMR experiments. It is known that during physical gelation, gelators are generally incorporated in a supramolecular solid-like network *via* non-covalent interactions, which causes line broadening, loss of spectral resolution, and peak disappearance in ^{1}H-NMR measurements.[60–62] This phenomenon was observed in a time-sweep ^{1}H-NMR experiment for $PBLG_{51}$ in toluene-d_8 over a few hours as well as in a temperature-sweep experiment for $P(BLG_{0.77}\text{-}co\text{-}LAG_{0.23})_{57}$

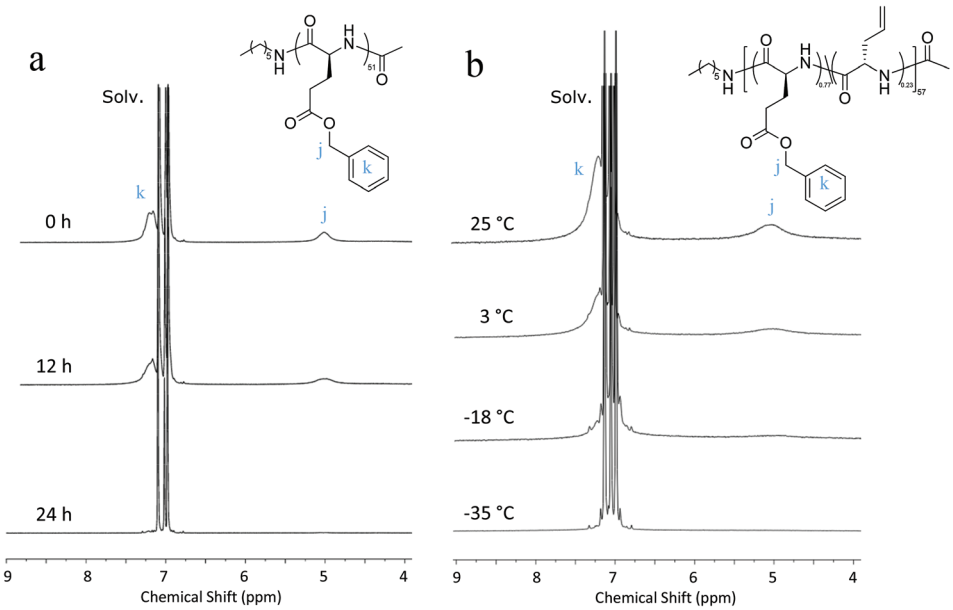

Fig. 3 ^{1}H-NMR (400 MHz) spectra of (a) homopolymer PBLG$_{51}$ in toluene-d$_8$ (4 g L^{-1}) at room temperature at 12 h intervals following dissolution of the polymer in toluene-d$_8$ at 60 °C for 1 h, and (b) copolymer P(BLG$_{0.77}$-*co*-LAG$_{0.23}$)$_{57}$ in toluene-d$_8$ (10 g L^{-1}) at different temperatures following dissolution of the polymer in toluene-d$_8$ at 60 °C for 1 h.

in toluene-d$_8$ below −18 °C (Fig. 3). This indicates that the gelation of P(BLG$_x$-*co*-AG$_{1-x}$)$_n$-toluene can be followed by ^{1}H-NMR, and that the melting point of P(BLG$_{0.77}$-*co*-LAG$_{0.23}$)$_{57}$-toluene 10 g L^{-1} gels is about −18 °C. It should be noted that, even before physical gelation, the ^{1}H-NMR spectra of our polymer-toluene-d$_8$ solutions did not show all chemical shifts normally observed in TFA-d solutions (Fig. S1a–S6a†), and the visible chemical shifts showed some level of line broadening. Based on the tendency for PBLG to exhibit an α-helical conformation and to aggregate in helicogenic solvents, we could explain this phenomenon by the fact that aggregates (fibers) already form at temperatures above gelation (causing line broadening) and grow as temperature decreases until the onset of physical gelation, which corresponds to a state where all aggregates are interconnected (causing peak disappearance). A cryo-rheometry study, which may help us determine the precise gelation temperatures of our gels, will be the topic of further research.

Photo-crosslinking gelation

We demonstrated that our P(BLG$_x$-*co*-AG$_{1-x}$)$_n$-toluene systems undergo physical gelation at low temperatures and that the percolated network, or gel microstructure, is composed of aggregated P(BLG$_x$-*co*-AG$_{1-x}$)$_n$ α-helices. In order to test our organogel-to-hydrogel route, the first step was to fix this physical gel network so that it can be preserved at room temperature, by crosslinking the allylglycine moieties using 1,9-nonanedithiol and benzophenone. UV-crosslinking by thiol–ene chemistry was selected as it is well known for being rapid (<1 h) and nearly quantitative.[56] Because we wanted to ensure that the physical gel network was preserved during the process, the P(BLG$_x$-*co*-AG$_{1-x}$)$_n$-toluene systems (5 to 50 g L^{-1}) were crosslinked at −77 °C (*i.e.*, below the gelation temperature of the systems and above the melting point of toluene). This cold crosslinking procedure was successful for P(BLG$_x$-*co*-AG$_{1-x}$)$_n$-toluene systems for which the proportion of AG is at least greater that 23% (*i.e.*, $1 - x > 0.23$), but failed for P(BLG$_{0.89}$-*co*-DLAG$_{0.11}$)$_{53}$-toluene systems. This is likely due to the fact that there is a minimum number of crosslinking moieties (*i.e.*, AG units) needed to readily fix and stabilize the gel microstructure. All crosslinked P(BLG$_x$-*co*-AG$_{1-x}$)$_n$-toluene gels showed partial shrinkage and a tendency to plastically deform when manipulated. This indicates that the gel microstructure of P(BLG$_x$-*co*-AG$_{1-x}$)$_n$-toluene systems is preserved by cold crosslinking are not load-bearing at room temperature.

To our surprise, UV-crosslinking of P(BLG$_{0.76}$-*co*-DLAG$_{0.24}$)$_{59}$-toluene (which does not physically gel) at −77 °C led to a gel. Similarly, UV-crosslinking of P(BLG$_x$-*co*-AG$_{1-x}$)$_n$-toluene systems at room temperature also led to gels. These room temperature-crosslinked gels, however, were found to be less mechanically stable than gels crosslinked at −77 °C (Fig. 4). This result indicates that our crosslinking procedure does not only fix an already interconnected physical gel or percolated network, formed in most P(BLG$_x$-*co*-AG$_{1-x}$)$_n$-toluene systems at −77 °C, but can also connect a more fluid, loosely bound network, expected to form in P(BLG$_x$-*co*-AG$_{1-x}$)$_n$-toluene systems at room temperature, thereby explaining why gels were obtained directly from dilute solutions upon crosslinking. This suggests that crosslinking of P(BLG$_x$-*co*-AG$_{1-x}$)$_n$ α-helices aggregated into a loosely bound network may be sufficient to yield gels even from dilute solutions. We thus named this

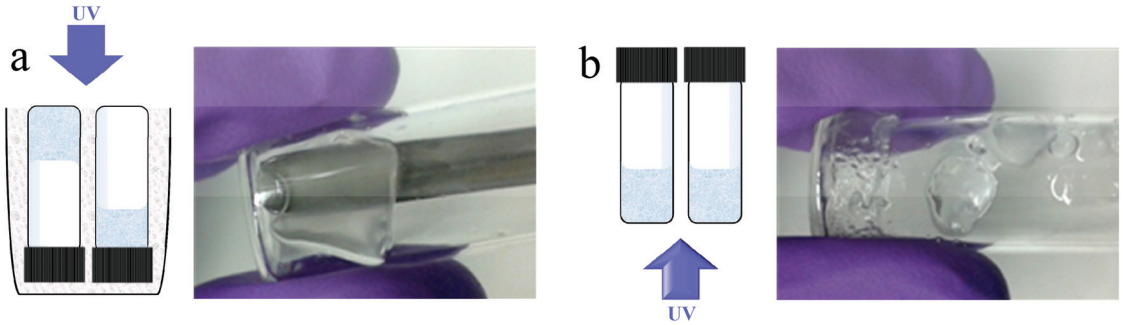

Fig. 4 (a) Crosslinking of P(BLG$_x$-*co*-AG$_{1-x}$)$_n$ in cooling bath (−77 °C) and typical gel with mild-compression resistance; the schematics depicts (left) P(BLG$_{0.77}$-*co*-LAG$_{0.23}$)$_{57}$-toluene (10 to 50 g L^{-1}) that forms a physical gel below −18 °C and remains set at the top (glass bottom) of the vial and (right) P(BLG$_{0.76}$-*co*-DLAG$_{0.24}$)$_{59}$-toluene (10 to 50 g L^{-1}) which does not form a physical gel and flows to the bottom (black lid) of the vial; (b) room temperature crosslinking of P(BLG$_x$-*co*-AG$_{1-x}$)$_n$ and typical gel with low-compression resistance.

crosslinking procedure photo-crosslinking gelation. This inspired us to explore room-temperature crosslinking of dilute solutions of P(BLG$_x$-*co*-AG$_{1-x}$)$_n$ in other helicogenic solvents. In particular, we focused on solvents in which PBLG is known to aggregate without physically gelling[46] in order to test the robustness of our photo-crosslinking gelation and better understand the mechanism.

We chose THF and dioxane since they promote aggregation of PBLG without gelation. Solutions of 10 g L^{-1} of P(BLG$_x$-*co*-AG$_{1-x}$)$_n$ in THF and in dioxane were successfully crosslinked in less than 20 min of UV exposure and yielded gels that showed almost no shrinkage and were mechanically strong (elastic response to mild compression). We thereby demonstrated that photo-crosslinking gelation can be achieved for dilute solutions of P(BLG$_x$-*co*-AG$_{1-x}$)$_n$ in different helicogenic solvents. This is an exceptional result as chemical gels from dilute solutions of low molar mass polymers (<50 000 g mol^{-1}) are unusual.[26] Dioxane gels were far superior to the toluene or THF based gels as they were mechanically robust and could be rapidly dried without collapsing the intricate gel microstructure formed (Fig. 5). For these reasons, P(BLG$_x$-*co*-AG$_{1-x}$)$_n$-dioxane systems were selected to investigate our organogel-to-hydrogel route.

Mechanism of photo-crosslinking gelation

In order to devise the most suitable organogel-to-hydrogel route, it was essential to understand how our copolymers self-assemble during the photo-crosslinking gelation mechanism and characterize their microstructure. First, let us consider the P(BLG$_x$-*co*-AG$_{1-x}$)$_n$-toluene systems, which underwent both physical gelation and photo-crosslinking gelation. The TEM micrographs of crosslinked P(BLG$_x$-*co*-AG$_{1-x}$)$_n$-toluene gels showed microstructures composed of interconnected high aspect ratio aggregates (Fig. 6) similar to the PBLG$_{51}$ fibers in physical gels (Fig. 1). By analogy with the mechanism by which PBLG physically aggregates and gels, it is likely that these fibrous aggregates result from the self-assembly of P(BLG$_x$-*co*-AG$_{1-x}$)$_n$ α-helices (Fig. 2) and that the level of aggregation (*e.g.*, aggregate size, concentration, or stiffness) increases with decreasing temperatures until physical gelation occurs, which is in good agreement with our ^{1}H-NMR studies (Fig. 3(b)). Based on this consideration, we postulate that our P(BLG$_x$-*co*-AG$_{1-x}$)$_n$

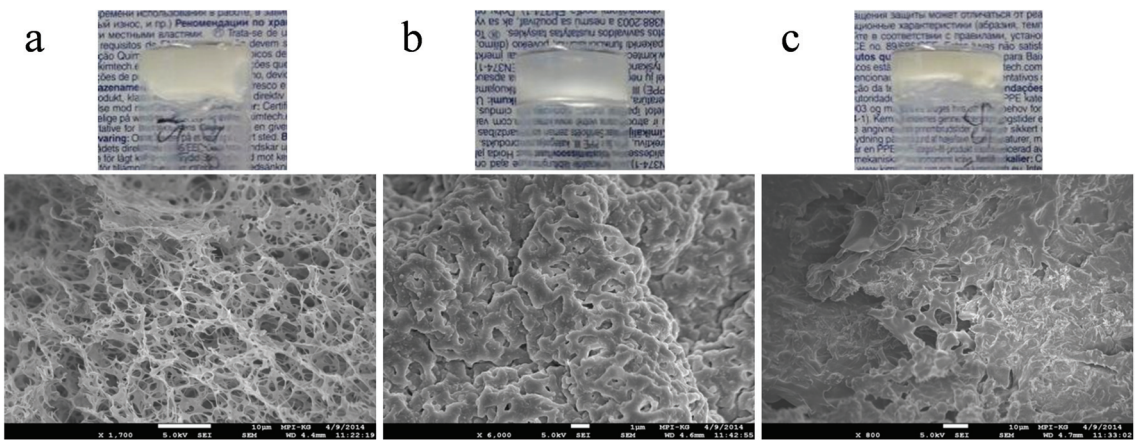

Fig. 5 SEM micrographs of typical freeze-dried 10 g L^{-1} organogels of P(BLG$_x$-*co*-AG$_{1-x}$)$_n$ in (a) 1,4-dioxane (scale bar = 10 μm), (b) toluene (scale bar = 1 μm) and (c) THF (scale bar = 10 μm); and vial inversion picture (above each micrograph).

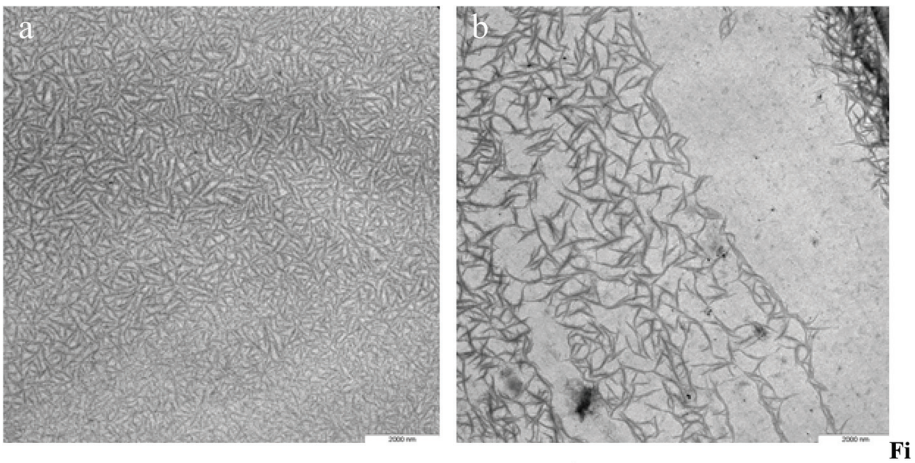

Fig. 6 Transmission electron micrographs of (a) 10 g L^{-1} P(BLG$_{0.76}$-*co*-DLAG$_{0.24}$)$_{59}$-toluene gel and (b) 5 g L^{-1} P(BLG$_{0.77}$-*co*-LAG$_{0.23}$)$_{57}$-toluene gel. Scale bars = 2000 μm.

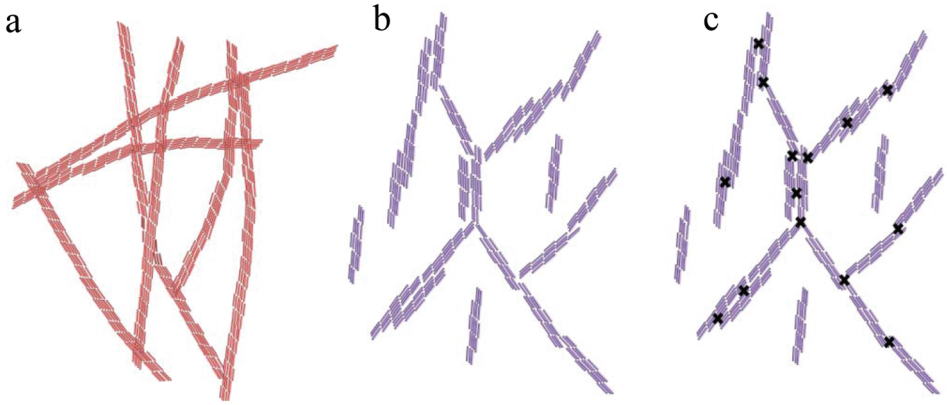

Fig. 7 Illustration of (a) the arrangement of PBLG helices into long fibers in toluene resulting in a percolation network, (b) postulated arrangement of P(BLG$_x$-*co*-AG$_{1-x}$)$_n$ helices into short fibers or high aspect ratio aggregates in dioxane and toluene, which are too short or unstable to generate a percolation network, (c) same system as b after UV-crosslinking (x) showing how a percolation network is generated.

copolymers fold into α-helices that self-assemble into fibrous aggregates over a broad temperature range including room temperature in helicogenic solvents (*e.g.*, THF, toluene, and dioxane) such that these aggregates can be covalently interconnected and fixed by UV-crosslinking of the AG moieties, without the need for physical gelation to occur. This fixation of the fibers leads to a percolated network of fibers, yielding our highly structured robust gels directly from dilute solutions (Fig. 7).

To test our hypothesis, we analyzed dilute solutions of P(BLG$_x$-*co*-AG$_{1-x}$)$_n$-dioxane by WAXS, and UV-crosslinked P(BLG$_x$-*co*-AG$_{1-x}$)$_n$-dioxane gels by high resolution SEM. We observed WAXS peaks at 2θ = 6–7° and 17°, corresponding to distances of 1.3–1.4 nm and 0.5 nm respectively, in lyophilized P(BLG$_x$-*co*-AG$_{1-x}$)$_n$-dioxane solutions (Fig. 8). The first peak can be assigned to a *d*-spacing of 1.3–1.4 nm corresponding to a pseudo-hexagonal packing of helices,[50,63,64] while the second 'peak', or shoulder, corresponds to the 0.5 nm helical pitch;[50] this indicates that P(BLG$_x$-*co*-AG$_{1-x}$)$_n$-dioxane and PBLG$_{51}$-dioxane aggregates have a similar microstructure. This result suggests that homopolymer PBLG$_{51}$ and statistical copolymer P(BLG$_x$-*co*-AG$_{1-x}$)$_n$ can both self-assemble in a similar fashion, that is pseudo-hexagonal packing of α-helices.

To confirm that such behavior results in the formation of fiber-like aggregates that can be preserved by UV-crosslinking, we analyzed our crosslinked gels by SEM. To do so, we dried crosslinked P(BLG$_x$-*co*-AG$_{1-x}$)$_n$-dioxane gels under high vacuum and analyzed their microstructure using high resolution SEM. We observed an interpenetrating fiber-like network (Fig. 5a). In order to ensure that such microstructure was not the result of lyophilization, since 1,4-dioxane freezes at 12 °C, we compared it to SEM micrographs of freeze-dried P(BLG$_x$-*co*-AG$_{1-x}$)$_n$-dioxane solutions (Fig. S8a–d†), which showed appreciably different features (*e.g.*, large open cell structure typical of freeze-

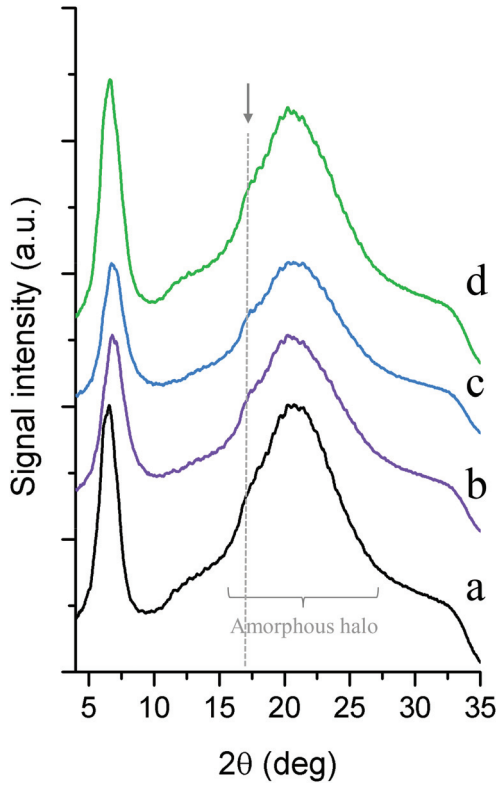

Fig. 8 Integrated wide-angle X-ray scattering patterns of freeze-dried P(BLG$_x$-*co*-AG$_{1-x}$)$_n$-dioxane solutions (20 g L^{-1}) showing an intense peak at 6–7° and a less intense peak at 17° (resolved by Levenberg–Marquardt curve-fitting); the amorphous halo is centered around 20–21°; (a) PBLG$_{51}$, (b) P(BLG$_{0.76}$-*co*-DLAG$_{0.24}$)$_{59}$, (c) P(BLG$_{0.77}$-*co*-LAG$_{0.23}$)$_{57}$, (d) P(BLG$_{0.89}$-*co*-DLAG$_{0.11}$)$_{53}$.

dried materials). These results validate the photo-crosslinking gelation mechanism for dilute solutions of P(BLG$_x$-*co*-AG$_{1-x}$)$_n$ as described above in our hypothesis. Interestingly, despite their low polymer concentration (down to 10 g L^{-1}), crosslinked P(BLG$_x$-*co*-AG$_{1-x}$)$_n$-dioxane gels were mechanically strong and behaved as solids for they did not flow and could be cut with a sharp knife; this is indicative of a particularly robust self-assembly, which is in line with previous studies on PBLG aggregation in helicogenic solvents.[43]

Debenzylation of the carboxylic acid moieties in dioxane-based organogels

As we showed that we were able to synthesize solid-like organogels consisting of a stable porous and fibrillar network formed by interconnected and crosslinked fibers, the next step was to investigate transitions from organogels to hydrogels. We focused on P(BLG$_x$-*co*-AG$_{1-x}$)$_n$-dioxane gels since their microstructure was sufficiently robust to sustain lyophilization (Fig. 5). Deprotection by cleavage of the benzyl group in P(BLG$_x$-*co*-AG$_{1-x}$)$_n$-dioxane gels yielded P(LG$_x$-*co*-AG$_{1-x}$)$_n$ hydrogels with high water content and with pH-responsive behavior. This deprotection was found to be more effective using hydrobromic acid (route B) than methanesulfonic acid (route A), as confirmed by ATR-FTIR with the lyophilized hydrogels (Fig. S9a and S9b†). Although a residual benzyl peak (<27% as calculated from ester ν(C=O) peak intensities of the normalized to amide II signal) could still be observed in our samples, this is unlikely to seriously impede the hydrogel performance. Despite the harsh debenzylation conditions, the gels showed no collapse and maintained their overall shape and volume.

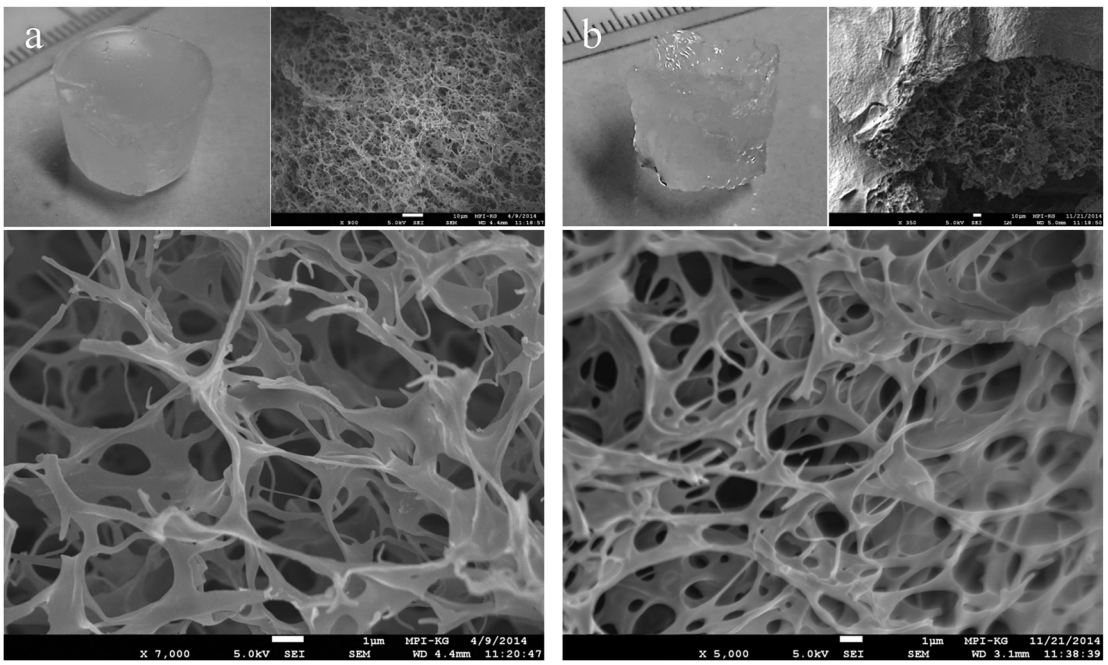

Fig. 9 SEM micrographs (a) dried P(BLG$_{0.76}$-*co*-DLAG$_{0.24}$)$_{59}$-dioxane organogel (10 g L^{-1}) and (b) freeze-dried P(LG$_{0.74}$-*co*-LAG$_{0.26}$)$_{170}$-water hydrogel (10 g L^{-1}); and corresponding pictures of (a) organogel and (b) hydrogel. Scale bars = 1 µm.

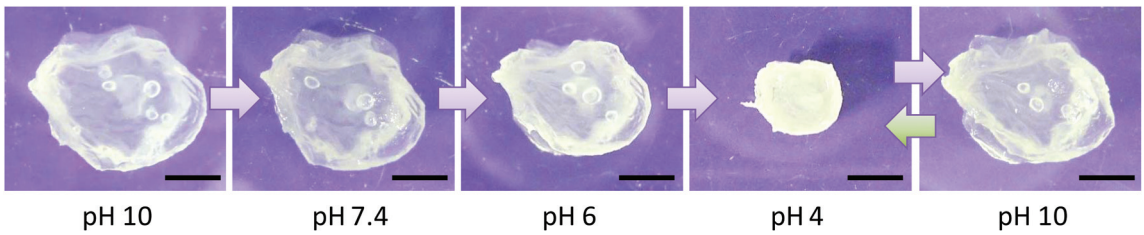

Fig. 10 P(LG$_{0.74}$-*co*-LAG$_{0.26}$)$_{170}$ hydrogel showing reversible pH-responsiveness; the scale bar is 5 mm.

This indicates that the porous microstructure observed in the organogel was preserved, as confirmed by SEM (Fig. 9).

We found that our hydrogels were able to hold up to 87 times their dry weight of water, which surpasses most PLGA-based hydrogels reported in the literature. More precisely, the swelling ratios (SR) of our 10 g L^{-1} gels ranged from 50 to 87, and the SR of our 20 g L^{-1} gels were lower, which is predictable with higher polymer-content gels, and ranged from 40 to 52 (Fig. S10†). The hydrogels were also tested for pH-responsiveness by submerging them in acidic and basic buffer solutions. They reversibly shrunk and swelled at pH 4 and at pH 10, respectively (Fig. 10). This behavior is caused by the pH-responsiveness of poly(L-glutamate) itself, which folds into hydrophobic α-helices below pH 6 (Fig. S11a and S11b†). While in the context of free polymers, such helices precipitate out of solution, in the context of gels, shrinkage takes place. This can be explained by the fact that hydrophobic poly(L-glutamic acid) helices undergo hydrophobic interaction, thereby causing the overall gel microstructure to reversibly contract. The shrinkage in acidic conditions took place within a few minutes, while the swelling in basic conditions took up to an hour to reach a fully swollen state. This discrepancy can be attributed to diffusion limitations in a shrunk gel. To confirm that the pH-driven coil-to-helix transition is responsible for the swelling-shrinking mechanism in P(BLG$_x$-*co*-AG$_{1-x}$)$_n$ hydrogels, Raman spectroscopy of these hydrogels was conducted at different pH. The Raman spectra clearly illustrate that the α-helical conformation dominates at pH 4, while random coil

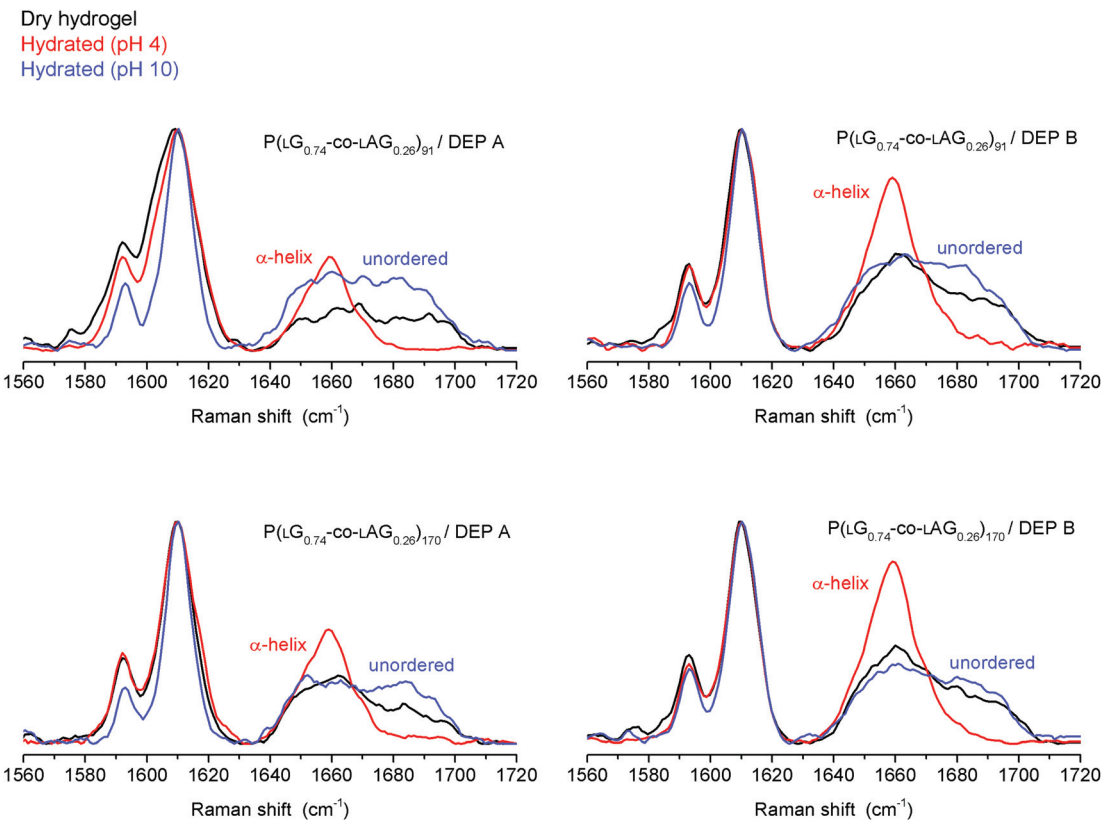

Fig. 11 Raman spectra of hydrogels (black) in their dry state, (red) following 2 h immersion in pH 4 buffer solution and (blue) following 2 h immersion in pH 10 buffer solution; upon base-line correction, normalization, smoothing and deconvolution (Levenberg–Marquardt algorithm); peak at 1658 cm^{-1} was assigned to an α-helical conformation, and two peaks at 1665 and 1683 cm^{-1} were assigned to an unordered conformation.[58]

conformation dominates at pH 10 (Fig. 11). In conclusion, our novel organogel-to-hydrogel route successfully produced high water content and pH responsive hydrogels that show reversible shrinkage-swelling behavior as pH varies.

Conclusion

We synthesized a series of high water content poly(L-glutamate) (PLG)/poly(L-glutamic acid) (PLGA) based hydrogels that showed reversible pH-responsiveness, which results from the helix-coil transition of the polypeptide chains below pH 6. Our hydrogels stand out from other reported PLGA gels as their swelling ratio in water, which reached 87, is greater than many PLGA-based chemical gels. In addition, unlike chemical and freeze-dried gels, their porous network is of fibrillar nature, which could lead the way towards a new generation of PLGA-based extracellular matrices for applications in regenerative medicine or even 3D cell culture. This was achieved by a novel route consisting of the self-assembly of statistical poly(γ-benzyl-L-glutamate-*co*-allylglycine) copolymers in dioxane followed by rapid photo-crosslinking gelation and subsequent deprotection of the carboxylic acid moieties. This organogel-to-hydrogel route is particularly unique in that it yields gels from dilute solutions (down to 10 g L^{-1}, *i.e.*, 1% w/v) of low molar mass polypeptides (down to 11 kg mol^{-1}). Remarkably, the resulting gels were mechanically robust, microfibrillar, and highly absorbing. We showed that this unique gelation pathway is driven by the self-assembly of our α-helical statistical copolymers into dynamic fiber-like aggregates, and that UV-crosslinking covalently interconnects these supramolecular assemblies, thereby forming a continuous solvent-trapping network and thus a robust gel. Due to their fibrillar and porous microstructure and inherent biocompatibility, these novel PLGA-based hydrogels represent excellent candidates for medical materials. Their pH-responsiveness and porosity mean that they could also be considered for medical materials in the context of cancers, viral, and other infectious diseases. Cytotoxic studies will be considered to that effect in the next stage of our study.

Acknowledgements

The authors would like to thank Marlies Gräwert (SEC), Rona Pitschke (TEM), and Jürgen Hartmann (TEM) (MPIKG) for their support and valuable contributions to this work. This work has been funded by the International Max Planck Research School (IMPRS) on "Multiscale Biosystems".

References

1 J. Huang and A. Heise, *Chem. Soc. Rev.*, 2013, **42**, 7373–7390.
2 A. S. Hoffman, *Adv. Drug Delivery Rev.*, 2013, **65**, 10–16.
3 C. Deng, J. Wu, R. Cheng, F. Meng, H.-A. Klok and Z. Zhong, *Prog. Polym. Sci.*, 2014, **39**, 330–364.
4 E. A. Appel, J. del Barrio, X. J. Loh and O. A. Scherman, *Chem. Soc. Rev.*, 2012, **41**, 6195–6214.
5 G. P. Raeber, M. P. Lutolf and J. A. Hubbell, *Biophys. J.*, 2005, **89**, 1374–1388.
6 L. Wei, C. Cai, J. Lin and T. Chen, *Biomaterials*, 2009, **30**, 2606–2613.
7 L. E. R. O'Leary, J. A. Fallas, E. L. Bakota, M. K. Kang and J. D. Hartgerink, *Nat. Chem.*, 2011, **3**, 821–828.
8 P. J. Flory, *Faraday Discuss. Chem. Soc.*, 1974, **57**, 7.
9 W. A. Petka, J. L. Harden, K. P. McGrath, D. Wirtz and D. A. Tirrell, *Science*, 1998, **281**, 389–392.
10 Q. Ye, G. Zünd, P. Benedikt, S. Jockenhoevel, S. P. Hoerstrup, S. Sakyama, J. A. Hubbell and M. Turina, *Eur. J. Cardio-Thorac. Surg.*, 2000, **17**, 587–591.
11 J. M. Berg, J. L. Tymoczko and L. Stryer, *Biochemistry*, W. H. Freeman and Company, New York, 6th edn, 2007.
12 D. I. Zeugolis, S. T. Khew, E. S. Y. Yew, A. K. Ekaputra, Y. W. Tong, L.-Y. L. Yung, D. W. Hutmacher, C. Sheppard and M. Raghunath, *Biomaterials*, 2008, **29**, 2293–2305.
13 T. J. Deming, *Soft Matter*, 2005, **1**, 28–35.
14 A. S. Hoffman, *Adv. Drug Delivery Rev.*, 2002, **54**, 3–12.
15 N. A. Peppas, P. Bures, W. Leobandung and H. Ichikawa, *Eur. J. Pharm. Biopharm.*, 2000, **50**, 27–46.
16 J. P. Jung, J. Z. Gasiorowski and J. H. Collier, *Biopolymers*, 2010, **94**, 49–59.
17 C. Zhao, X. Zhuang, P. He, C. Xiao, C. He, J. Sun, X. Chen and X. Jing, *Polymer*, 2009, **50**, 4308–4316.
18 Y. Matsuoka, R. Kishi and M. Sisido, *Polym. J.*, 1993, **25**, 919–927.
19 K. Inomata, Y. Iguchi, K. Mizutani, H. Sugimoto and E. Nakanishi, *ACS Macro Lett.*, 2012, **1**, 807–810.
20 S. Murakami, N. Aoki and S. Matsumura, *Polym. J.*, 2011, **43**, 414–420.
21 Y.-H. Lee, J.-J. Chang, W.-F. Lai, M.-C. Yang and C.-T. Chien, *Colloids Surf., B*, 2011, **86**, 409–413.
22 J. Zou, F. Zhang, Y. Chen, J. E. Raymond, S. Zhang, J. Fan, J. Zhu, A. Li, K. Seetho, X. He, D. J. Pochan and K. L. Wooley, *Soft Matter*, 2013, **9**, 5951.
23 C.-M. Dong and Y. Chen, *J. Controlled Release*, 2011, **152**, e13–e14.
24 T. J. Deming, *Adv. Mater.*, 1997, **9**, 299–311.
25 H. Kukula, H. Schlaad, M. Antonietti and S. Förster, *J. Am. Chem. Soc.*, 2002, **124**, 1658–1663.
26 W. T. Truong, Y. Su, J. T. Meijer, P. Thordarson and F. Braet, *Chem. – Asian J.*, 2011, **6**, 30–42.
27 J.-F. Lutz, M. Ouchi, D. R. Liu and M. Sawamoto, *Science*, 2013, **341**, 1238149.
28 H. Block, *Poly(gamma-benzyl-L-glutamate) and other glutamic acid containing polymers*, Gordon and Breach Science Publishers Ltd., 1983.
29 J. P. Tam, W. F. Heath and R. B. Merrifield, *J. Am. Chem. Soc.*, 1983, 6442–6455.
30 M. Idelson and E. R. Blout, *J. Am. Chem. Soc.*, 1958, **80**, 4631–4634.

31 Y. Kato and Y. Tsukadat, *J. Med. Chem.*, 1984, **27**, 1602–1607.
32 J. Cheng and T. J. Deming, *Top. Curr. Chem.*, 2012, **310**, 1–26.
33 C. W. Song, R. Griffin and H. J. Park, in *Cancer Drug Resistance*, ed. B. Teicher, Humana Press Inc., 2006, pp. 21–43.
34 Y. Kato, S. Ozawa, C. Miyamoto, Y. Maehata, A. Suzuki, T. Maeda and Y. Baba, *Cancer Cell Int.*, 2013, **13**, 1–8.
35 L. G. Barrientos and P. E. Rollin, *Virology*, 2007, **358**, 1–9.
36 A. Lardner, *J. Leukocyte Biol.*, 2001, **69**, 522–530.
37 F. Chécot, S. Lecommandoux, Y. Gnanou and H.-A. Klok, *Angew. Chem., Int. Ed.*, 2002, **114**, 1395–1399.
38 C. Zhao, P. He, C. Xiao, X. Gao, X. Zhuang and X. Chen, *J. Appl. Polym. Sci.*, 2012, **123**, 2923–2932.
39 Z. Yang, Y. Zhang, P. Markland and V. C. Yang, *J. Biomed. Mater. Res.*, 2002, **62**, 14–21.
40 J. Rodríguez-Hernández and S. Lecommandoux, *J. Am. Chem. Soc.*, 2005, **127**, 2026–2027.
41 K.-S. Krannig and H. Schlaad, *J. Am. Chem. Soc.*, 2012, **134**, 18542–18545.
42 L. A. Estroff and A. D. Hamilton, *Chem. Rev.*, 2004, **104**, 1201–1218.
43 R. Sakamoto, *Colloid Polym. Sci.*, 1984, **262**, 788–792.
44 Y. Izumi, H. Takezawa, N. Kikuta, S. Uemura and A. Tsutsumi, *Macromolecules*, 1998, **31**, 430–435.
45 R. Tadmor, R. L. Khalfin and Y. Cohen, *Langmuir*, 2002, 7146–7150.
46 C. L. Jackson and M. T. Shaw, *Polymer*, 1990, **31**, 1070–1084.
47 K. Tohyama and W. G. Miller, *Nature*, 1981, **289**, 813–814.
48 J. C. Horton and A. M. Donaldt, *Polymer*, 1991, **32**, 2418–2427.
49 S. Chakrabarti and W. G. Miller, *Biopolymers*, 1984, **23**, 719–734.
50 A. Niehoff, A. Mantion, R. McAloney, A. Huber, J. Falkenhagen, C. M. Goh, A. F. Thünemann, M. F. Winnik and H. Menzel, *Colloid Polym. Sci.*, 2013, **291**, 1353–1363.
51 K. T. Kim, C. Park, G. W. M. Vandermeulen, D. A. Rider, C. Kim, M. A. Winnik and I. Manners, *Angew. Chem., Int. Ed.*, 2005, **44**, 7964–7968.
52 S. S. Naik and D. A. Savin, *Macromolecules*, 2009, **42**, 7114–7121.
53 Y. Yamane, M. Kanekiyo, S. Koizumi, C. Zhao, S. Kuroki and I. Ando, *J. Appl. Polym. Sci.*, 2004, **92**, 1053–1060.
54 J. Huang, G. Habraken, F. Audouin and A. Heise, *Macromolecules*, 2010, **43**, 6050–6057.
55 K.-S. Krannig, J. Sun and H. Schlaad, *Biomacromolecules*, 2014, **15**, 978–984.
56 S. M. Brosnan and H. Schlaad, *Polymer*, 2014, **55**, 5511–5516.
57 D. L. Tipton and P. S. Russo, *Macromolecules*, 1996, **9297**, 7402–7411.
58 E. C. Y. Li-Chan, A. A. Ismail, J. Sedman and F. R. Van de Voort, *Handbook of Vibrational Spectroscopy*, ed. J. M. Chalmers and P. R. Griffiths, Wiley, 2001, p. 4345.
59 R. M. Guinn, A. O. Margot, J. R. Taylor, M. Schumacher, D. S. Clark and H. W. Blanch, *Biopolymers*, 1995, **35**, 503–512.
60 G. Yu, X. Yan, C. Han and F. Huang, *Chem. Soc. Rev.*, 2013, **42**, 6697–6722.
61 Y. E. Shapiro, *Prog. Polym. Sci.*, 2011, **36**, 1184–1253.
62 X. Yan, D. Xu, X. Chi, J. Chen, S. Dong, X. Ding, Y. Yu and F. Huang, *Adv. Mater.*, 2012, **24**, 362–369.
63 K. Jahanshahi, I. Botiz, R. Reiter, R. Thomann, B. Heck, R. Shokri, W. Stille and G. Reiter, *Macromolecules*, 2013, **46**, 1470–1476.
64 A. J. McKinnon and A. V. Tobolsky, *J. Phys. Chem.*, 1968, **72**, 1157–1161.